Journal of Structural Geology, Vol. 10, No. 2, pp. 155 to 170, 1988
Printed in Great Britain

0191-8141/88 $03.00 + 0.00

Relations between normal-fault geometry, tilting and vertical motions in extensional terrains: an example from the southern Gulf of Suez

J. A. JACKSON,* N. J. WHITE,* Z. GARFUNKEL† and H. ANDERSON*‡

*Bullard Laboratories, Department of Earth Sciences, University of Cambridge, Madingley Rise, Madingley Road, Cambridge CB3 0EZ, U.K. and †Department of Geology, the Hebrew University, Jerusalem, Israel

(*Received* 29 *June* 1987; *accepted in revised form* 25 *October* 1987)

Abstract—Earthquakes and data from subsurface oil exploration suggest that large active normal faults in the southern Gulf of Suez are approximately planar, with dips of 30–40°, from the surface to around 10 km depth. These faults, and the blocks they bound, appear to rotate about a horizontal axis as they move, causing tilting. This tilting is seen both in young vertical movements of the coastline, such as raised beaches and marshlands, and in the distribution of Middle Miocene marine rocks, which are uplifted to elevations of 400–500 m in footwalls of faults and found at depths of around 3500 m in the adjacent grabens. The absolute amplitude of the observed vertical motions can be approximately modelled by planar rotating normal faults that impose a saw-tooth topography on a regional subsidence caused by crustal and lithospheric thinning. The observations required for this simple model are: the present day fault dip, the amount of tilting and the width of the rotating blocks. The virtues of the model are its simplicity and its compatibility with our knowledge of how large active normal faults move elsewhere on the continents.

INTRODUCTION

THE PURPOSE of this paper is to investigate the relations between vertical movements and the geometry of large normal faults in regions of continental extension. Vertical movements relative to an absolute datum, such as sea level, are known to accompany normal faulting, and, since such movements control the geomorphology and drainage in regions of extension, an ability to predict quantitatively the amplitude and distribution of these movements is of obvious importance in understanding the sedimentary history of a basin. Our approach to this problem will be to use our knowledge of how large active normal faults move to try and predict the longer-term finite displacements seen in the geological record. Active normal faults that move during large earthquakes may be studied using both seismological techniques and surface observations. These are able to constrain the three-dimensional geometry of the fault and, if a pre-earthquake horizontal reference level is available (from geodetic measurements or sea level), the absolute vertical movements associated with faulting can also be observed. Perhaps surprisingly, large active normal faults that are studied in this way reveal a simple pattern to their kinematics and geometry that can be generalized and used as a predictive tool: our knowledge of large seismogenic normal faults is briefly summarized in the next section. We will then apply this understanding to the southern Gulf of Suez, which is a region of currently active extension that has also been explored by oil companies. Subsurface information is therefore available from both hydrocarbon exploration and earthquake seismology, and the presence of the sea provides a reference level against which to estimate vertical movements.

LARGE ACTIVE NORMAL FAULTS

Within the last 10 years it has become possible to estimate earthquake focal depths to an accuracy (±3 km or better in some circumstances) that is geologically useful. In general, earthquakes occur in only the upper part of the continental crust— the lower part remains aseismic. The observed lower limit to focal depths is often abrupt and occurs at a level that varies with regional heat flow. The seismic–aseismic transition is thus thought to be temperature-controlled and to separate an upper ('brittle') seismogenic crust, in which deformation is by frictional sliding on faults, from a lower ('ductile') aseismic crust where deformation occurs by creep or flow. The depth of the transition is typically in the range 8–15 km, and probably occurs at temperatures in the range 350 ± 100°C. This interpretation of the focal depth distribution is qualitatively in agreement with laboratory experiments of rock deformation. The summary above is of work pioneered by Sibson (1982), Meissner & Strehlau (1982) and Chen & Molnar (1983). An important additional observation is that the largest earthquakes in a region, particularly those whose faults break the surface, tend to have focal depths at the base of the seismogenic layer (Eyidoğan & Jackson 1985, Strehlau 1986), and so involve rocks that would usually be designated 'basement'. This layer therefore imposes a fundamental scale on faulting because faults (and earthquakes) have dimensions that are either small, or are comparable to its thickness: a view that has concerned seismologists for some time (e.g. Scholz 1982, Shimazaki 1986) but is probably less well known among structural geologists. Here, we are concerned only with seismogenic normal faults that are

‡Present address: DSIR (Geophysics Division), P.O. Box 1320, Wellington, New Zealand.

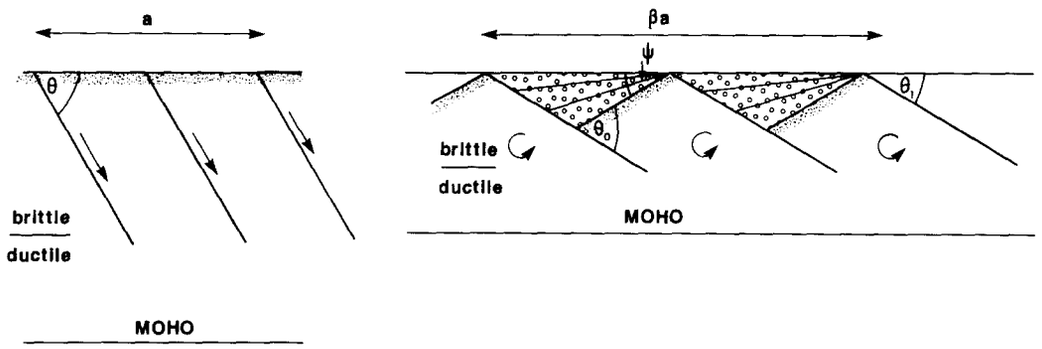

Fig. 1. Cartoon sections to illustrate the rotating block ('domino') style of extension. Faults start with a dip θ_0, then tilt through an angle ψ to attain a new dip θ_1. The surface area increases by a factor of β. Note that the sediments infilling the graben show growth towards the fault. We do not draw faults below the seismic–aseismic ('brittle–ductile') transition, which we show to be raised by the extension. Whether the transition is actually raised depends primarily on the extensional strain rate (see England & Jackson 1987).

large or comparable to the thickness of the upper crust. Such faults move in earthquakes of magnitude 5.5 or greater and reveal a simple pattern: their fault plane solutions show that their dip at the base of the brittle crust is almost always in the range 30–60° (Jackson 1987). Moreover, where observational control is good, these faults appear to be approximately planar (within 10–20°) from their nucleation point near the seismic–aseismic transition to the surface (Eyidoğan & Jackson 1985, Stein & Barrientos 1985). Smaller earthquakes show no such regularity: their fault plane solutions may be extremely varied and they probably represent internal deformation of blocks bounded by large faults. Although more numerous, the cumulative effect of small earthquakes can often be shown to account for much less strain that the movement in large earthquakes (see Westaway & Jackson 1987).

Both tilting and vertical movements are observed to accompany movement on active normal faults. Vertical movements involve uplift of the footwall and subsidence of the hangingwall blocks and can be observed either geodetically (Jankhof 1945, Richter 1958, Myers & Hamilton 1964, Savage & Hastie 1966, Stein & Barrientos 1985) or by reference to sea level (Jackson *et al.* 1982). These vertical movements decrease with distance from the fault and thus lead to a tilting of the footwall and hangingwall blocks. The fault consequently rotates about a horizontal axis so as to reduce its dip. These observations may be interpreted in several ways that are not mutually exclusive. The vertical motions accompanying movement on a single normal fault may be seen as either the effect of elastic rebound immediately following fault slip (e.g. Savage & Hastie 1966, Stein & Barrientos 1985), or in the longer term, as an isostatic and flexural response to the unloading of the footwall (Jackson & McKenzie 1983). However, normal faults rarely occur in isolation, but are commonly distributed across zones in which several sub-parallel faults dip in the same direction. Thus a single block is likely to be both the footwall of one fault and the hangingwall of another. The vertical movements imposed on the block by its two bounding faults therefore amount to a torque requiring the block to rotate about a horizontal axis, so as to reduce the dip of the faults. This kinematic evolution is the familiar 'rotating domino' style of extension (Ransome *et al.* 1910), which can be considered as the achievement of overall pure shear (crustal extension and thinning) by simple shear (faulting) and rotation (see Fig. 1 and Jackson 1987). Seismological observations support this simple model of extension in that the large earthquake-generating normal faults that cut right through the brittle upper crust are observed to be approximately planar and to rotate as they move. Moreover, they tend to occur in zones containing several sub-parallel faults that dip and tilt the same way (e.g. Garfunkel & Bartov 1977, Stewart 1980, Jackson & McKenzie 1983). This model suggests a simple explanation for the restricted range of observed dips of large active normal faults: that such faults start to move at dips no steeper than 60° and rotate until they reach a dip of 30° (Jackson 1987).

In this paper we will discuss quantitative relations between fault geometry, tilting and vertical movements using this simple rotating domino model, but before doing so we will first try to dispel some common misconceptions about this model.

The first is the belief that the bases or keels of the rotating blocks represent a space problem (e.g. Gibbs 1984). In the case of the large normal faults that concern us here, which break right through the brittle upper crust, this belief arises from a misunderstanding of the nature of the seismic–aseismic transition. This transition is likely to be a temperature horizon, and so neither compositional nor fixed to the rotating blocks. A horizontal section through the keels of the tilted blocks would show a saw-tooth perturbation to the temperature with a periodicity of L, where L is the spacing of the blocks, and zero perturbations separated by a distance $0.5L$. This change to the thermal structure will decay with a time constant of $L^2/4\pi^2\kappa$, where κ is the thermal diffusivity (about 10^{-6} m^2 s^{-1}). For blocks 25 km apart this time constant is about 0.5 Ma; unless the extension occurs quickly compared with this time, the seismic–aseismic transition will not be perturbed significantly by block movement. Because the seismic–aseismic transition is not a material horizon, there is no need for a

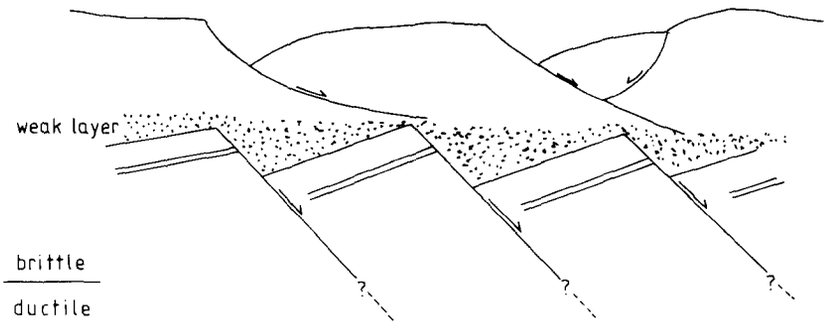

Fig. 2. Schematic cartoon to show how a lithologically weak layer (e.g. overpressured shale or salt) may allow the extension in the sediments above to be decoupled from the fault-bounded tilted blocks in the basement below.

subhorizontal 'detachment' or 'décollment' zone of discrete slip at the base of the tilted blocks.

Another misconception is that 'growth' in the hangingwall sediments of a normal fault (i.e. an increase in stratigraphic thickness towards the fault) requires that the fault be 'listric' (i.e. flatten with depth), rather than planar. This is not the case if the fault concerned rotates about a horizontal axis as it moves: syn-faulting sediments will then exhibit growth geometries, as illustrated schematically in Fig. 1. There is no doubt that normal faults with listric geometries, that flatten in the brittle upper crust, do exist. In many cases they flatten at lithologically controlled depths onto weak layers such as overpressured shale or evaporites. However, there is no evidence that they generate large earthquakes (Jackson 1987). The role of such listric faults often appears to be to redistribute the sedimentary cover in response to surface topography. In some cases, such as the Gulf of Mexico (e.g. Garrison & Martin 1973) basement extension is not involved. In others, faulting within the sedimentary cover may be decoupled from domino-style fault-bounded blocks in the basement by a weak layer into which the sedimentary faults flatten. Such a geometry may be applicable to the central North Sea (e.g. Gibbs 1984) and is illustrated schematically in Fig. 2.

THE GULF OF SUEZ

General geology

The Gulf of Suez is a 400 km long Cenozoic rift separating the Sinai peninsula from mainland Africa. Early summaries of its history and structure by Said (1962), Robson (1971) and Garfunkel & Bartov (1977) have been supplemented by more recent accounts of its stratigraphic development by Chenet & Letouzey (1983), Selwood & Netherwood (1984), Angelier (1985), Moretti & Colletta (1987, 1988) and Colletta *et al.* (in press) among others. Only the briefest summary is needed here.

The region contains a Precambrian metamorphic and granitic basement that was overlain by continental and marine sediments of Cambrian to Eocene age and started to break up in late Oligocene times. The initiation of rifting was accompanied by widespread, but volumetrically minor, basaltic volcanism. Marine sedimentation apparently started in the early Miocene (Aquitanian to Burdigalian) and consists of some clastic material but mostly of evaporites and marls. The structure of the rift is dominated by normal faults and tilted blocks trending NW–SE, with sedimentary fill locally up to 6 km thick. Much of the present structure was outlined by the end of the early Miocene (about 15 Ma). The uplifted edges of many tilted blocks were then eroded, but they were subsequently overlain unconformably by younger Miocene beds. Still later, the central part of the rift, consisting mainly of the area now under the sea, continued to subside. Continuing fault motion is clear from numerous scarps that displace young alluvium on the rift margins, and from earthquakes. Under the Gulf, continued block motion is recorded by thickness variations in Quaternary sediments and by mild relief of the Gulf floor where young sedimentation did not keep pace with faulting.

This paper is concerned with the southern part of the Suez rift, which is still seismically active (Figs. 3–5). Here the structure is asymmetric with most large blocks tilted to the SW and their bounding faults dipping NE. A major NE-dipping fault, or series of en échelon faults, here called the Zeit–Shadwan Fault, bounds the western side of the strongly subsided central part of the Gulf. The footwall of this fault is a row of high standing tilted blocks extending from Gebel Zeit to Shadwan Island. The Gebel Zeit block exposes the Precambrian basement on its uplifted edge and pre-rift sediments that are tilted by more than 35° (Perry 1983, Angelier 1985, Moretti & Colletta 1988, Colletta *et al.* in press), which is a high value for the Suez rift. Along the high edge of Gebel Zeit, Middle Miocene marine rocks dipping 10–15° SW overlie pre-rift rocks with an angular unconformity (Fig. 6b), showing that considerable tilting had already occurred by this time. South-west of Gebel Zeit the next major NE-dipping fault bounds another basement ridge called Esh Melaha. In the southern part of this ridge (near 27.4°N) a Miocene platform of carbonate–siliciclastic deposits is preserved on top of the basement and is tilted gently (2–5°) to the SW. A spectacular sedimentary talus preserves the morphology of the normal fault on the NE flank of the plateau (El Haddad *et al.* 1984, Aissaoui *et al.* 1986), but further

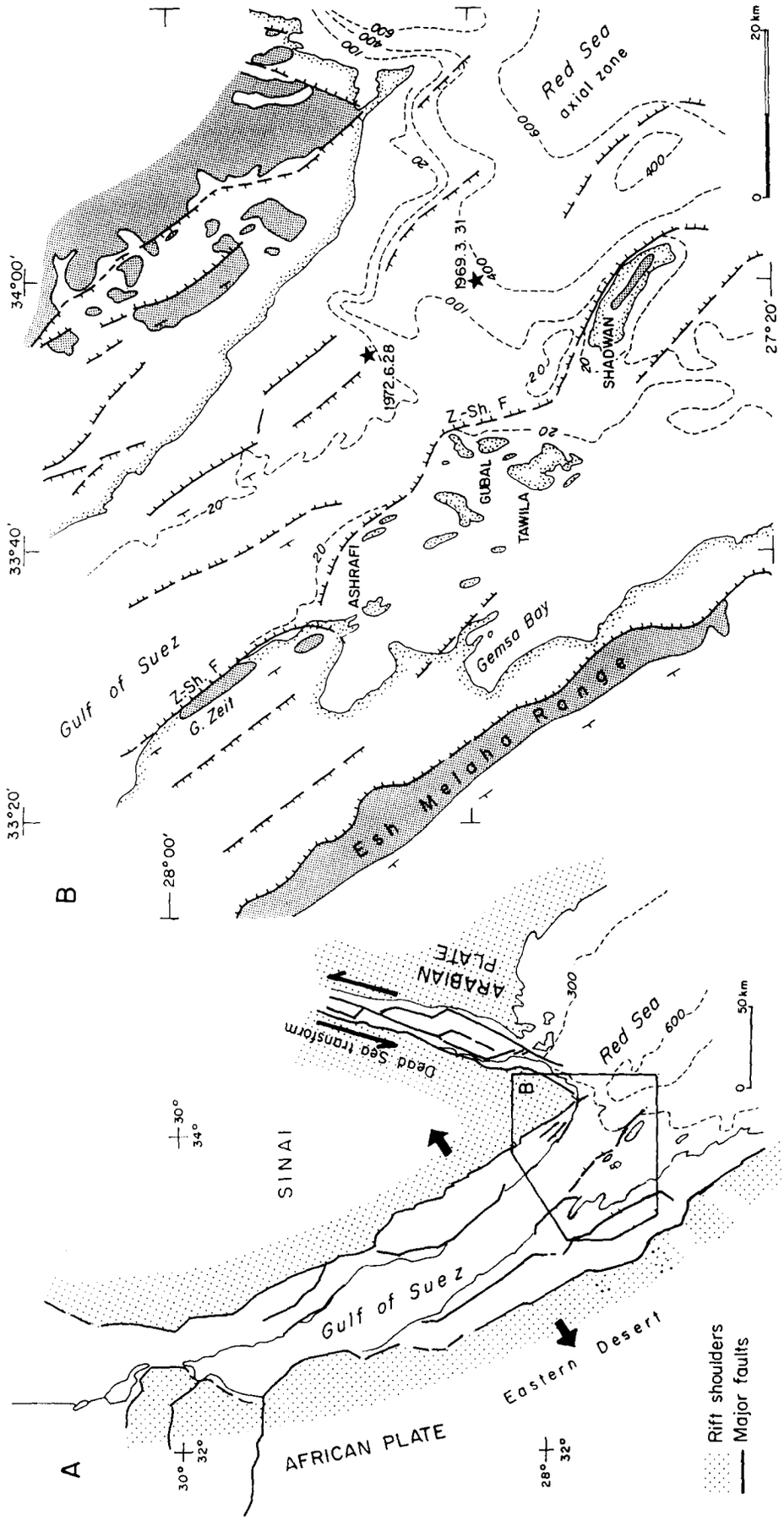

Fig. 3. (a) Major structures of the Suez rift. Arrows indicate the approximate direction of separation between Sinai and Africa. (b) Detailed map of the region marked B in Fig. 3(a) (see also Fig. 5). Outcrops of Precambrian basement are stippled. Major faults are shown by heavy lines with ticks on the downthrown side. Z–Sh.F: Zeit–Shadwan Fault. Bathymetry is in fathoms. Stars are the approximate epicentres of the 21 March 1969 and 28 June 1972 earthquakes (see text).

Fig. 5. Landsat image of the Gebel Zeit–Esh Melaha region (see Fig. 3b). Dark rocks outcropping on Gebel Zeit and Esh Melaha are Precambrian basement, bounded on their NE sides by abrupt fault escarpments. Note the dark marshy area on the NW coast of Zeit Bay.

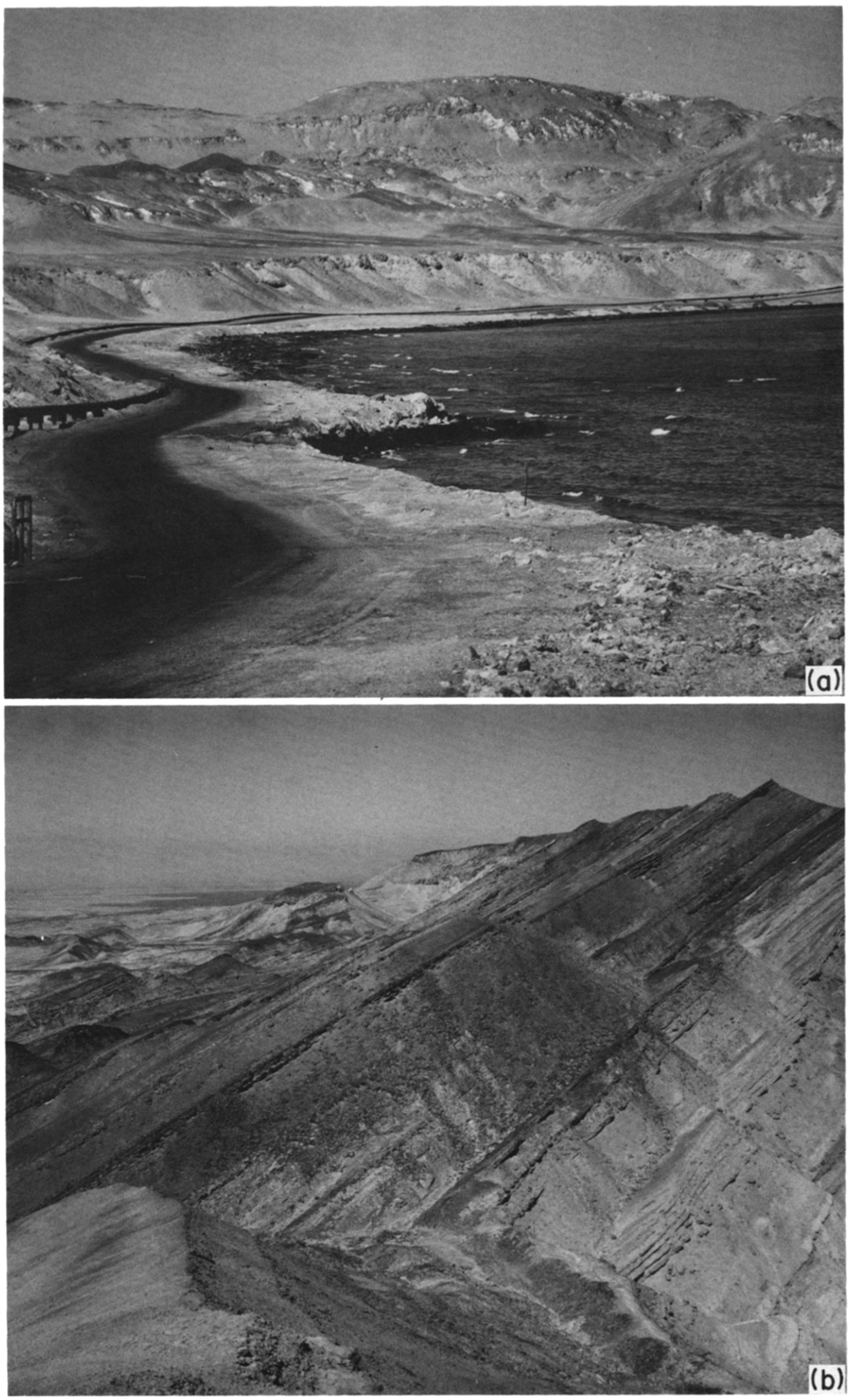

Fig. 6. (a) The shoreline at the northern end of Gebel Zeit, looking W. The road is on a raised beach at 2–3 m elevation. A higher beach terrace, with hard corals that resist erosion, is at an elevation of about 8 m. Elsewhere on this coast additional higher terraces are present, but poorly preserved. (b) View looking NW along the SW side of Gebel Zeit at its northern end. In the foreground, pre-Miocene rocks are tilted 35° towards the SW. On the centre skyline are Middle Miocene sediments dipping 10–15°SW, which unconformably overlie the older rocks in the foreground.

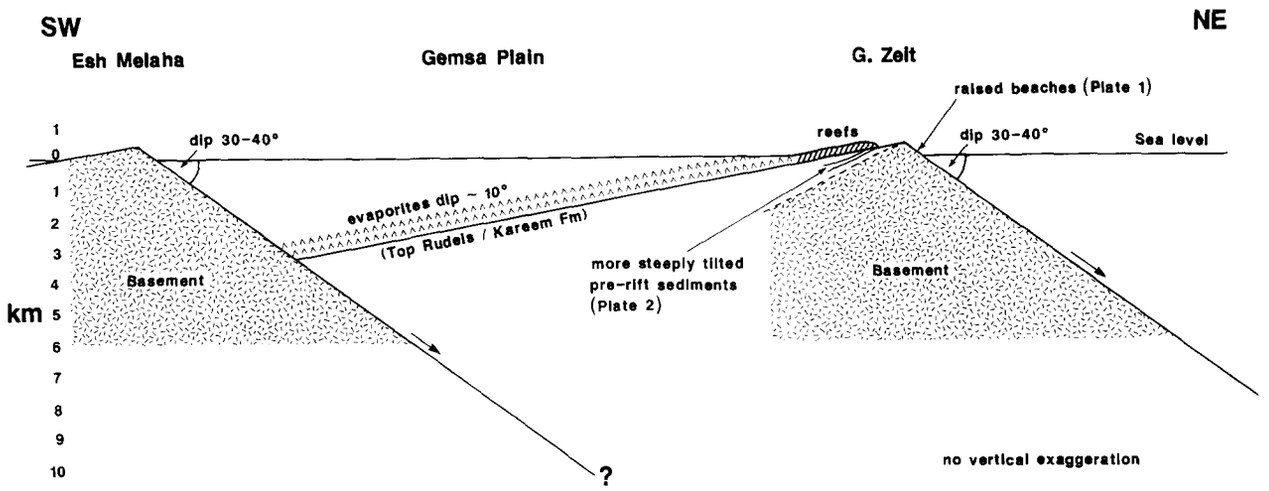

Fig. 4. Schematic cross-section through the Esh Melaha and Gebel Zeit blocks (after Perry 1983 and others). The geology has been greatly simplified and omits some antithetic faulting dipping SW. Because of differential compaction, a uniform dip at the base of the evaporites is unlikely immediately in front of the Esh Melaha Fault: a gentle hangingwall syncline is more probable.

north, at the latitude of Gebel Zeit, the platform itself is not preserved.

Vertical movements

Signs of Quaternary uplift are common in the southern Gulf of Suez. Raised beaches and marine terraces up to 80 m above sea level are seen along the NE flank of Gebel Zeit (Fig. 6a and Moretti & Colletta 1988, Colletta *et al.* in press). Raised beaches are also seen on the NE coasts of the islands of Gubal (Crossland 1939) and Shadwan (Shukri 1954). All these sites are in the footwall of the Zeit–Shadwan Fault. Terraces are absent or lower on the SW side of Gebel Zeit, which at its SE end is covered by marshlands at sea level on the SW side, attesting to continued tilting of the Gebel Zeit block (Garfunkel & Bartov 1977, Colletta *et al.* in press).

Middle Miocene marine rocks dipping 10–15° outcrop at elevations of about 300 m above sea level on the SW flank of Gebel Zeit and may have once covered the whole mountain, whose current maximum elevation is about 465 m. These same sediments are found at depths of 3500 m beneath the Gemsa Plain in the hangingwall of the Esh Malaha Fault (Perry 1983). This is compatible with the block bounded by the Esh Melaha and Gebel Zeit Faults having rotated about 10° as a relatively rigid block in the last 10 Ma (Perry 1983, Colletta *et al.* in press). A schematic cross-section through Gebel Zeit and Esh Melaha is shown in Fig. 4. The question of interest here is how the faulting and tilting in this region lead to the observed vertical motions of the Middle Miocene sediments.

It is important to bear in mind that some of the vertical movement seen in the Gulf of Suez is likely to be part of a long wavelength uplift of the entire region, and may be dynamically related to the cause of the rifting itself (see Moretti & Froidevaux 1986, Steckler 1986, Moretti *et al.* 1987). However, superimposed on this regional uplift are the shorter wavelength vertical motions associated with normal faulting, which are not only to be expected (see next section), but are clear from the association of both present day uplift and subsidence with the location of major active faults (Moretti & Colletta 1987, 1988).

Fault geometry

The morphology of large faults in the southern Gulf of Suez is rarely well preserved at the surface as the basement rocks erode very easily. Nevertheless, fieldwork and some subsurface data suggest that the largest normal faults (like the Zeit–Shadwan Fault), which bound blocks tilted 20–30°, dip in the range 30–45° near the surface (Colletta *et al.* in press), with the angle between the major faults and the pre-rift bedding about 50–65° (Chenet *et al.* 1985). Drilling offshore from Gebel Zeit suggests that the main NE-dipping Gebel Zeit Fault dips in the region of 30–40° in the top 3 km (Letouzey personal communication). These observations are consistent with the major faults initiating at a near-surface dip of about 60° and rotating to flatter dips.

The deeper structure of the main normal faults is not known from seismic reflection data, which generally reveal few coherent reflections beneath the great thickness of Miocene salt. However, two large recent normal faulting earthquakes occurred in this part of the Gulf of Suez, and seismological analysis is able to reveal the orientations and depths of the faults on which they occurred.

The first, on 31 March 1969, of magnitude (Ms) 6.8, had an epicentre offshore in the southern part of the Gulf (Fig. 7). The earthquake caused much fissuring and slumping on Shadwan Island (Maamoun & El-Kashab 1978) with some cracks more than 1 km long. There were no unequivocal reports of surface faulting, and no reports of faulting with a length (about 15 km) and displacement (about 1–2 m) expected from an earthquake of this size. The fault plane solution of this earthquake indicates normal faulting with a NW strike dipping either NE (at about 35°) or SW (at about 55°). All the large faults in this region dip NE and it is

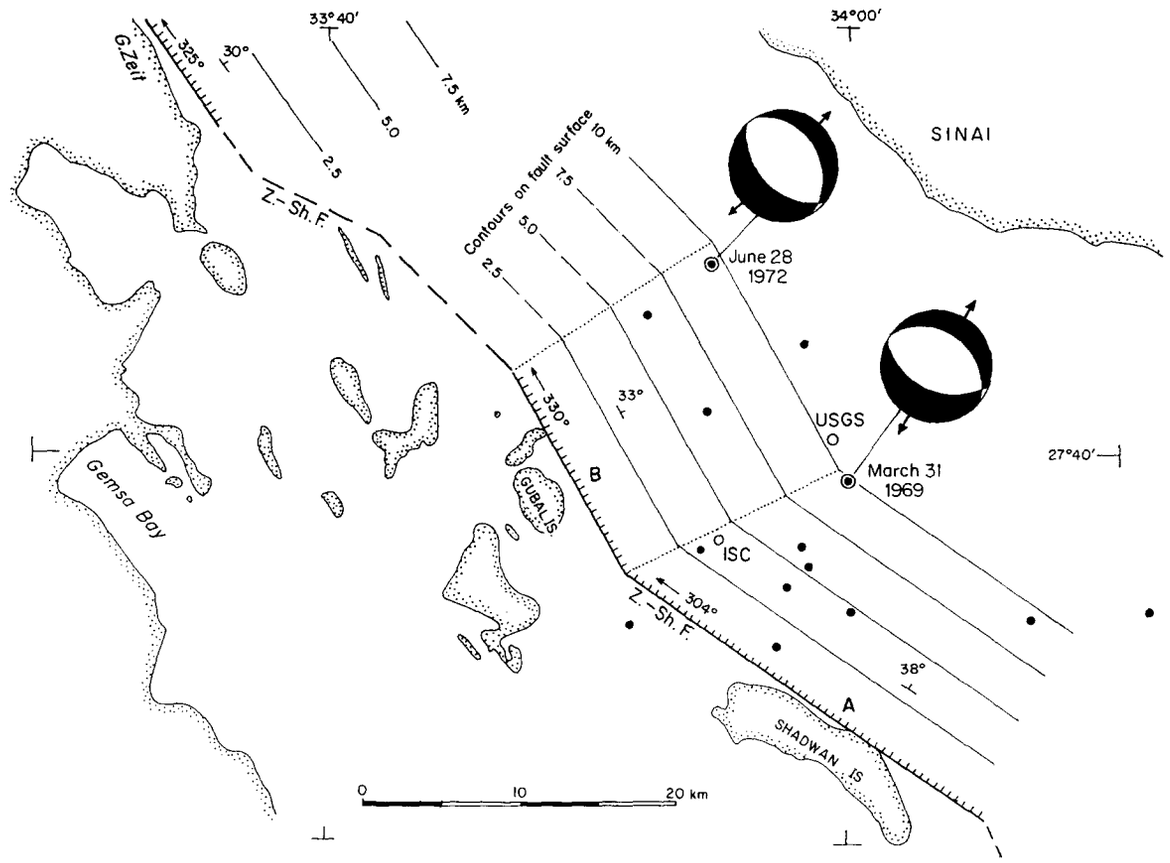

Fig. 7. Map to show our preferred epicentres and focal mechanisms for the earthquakes of 21 March 1969 and 28 June 1972. Black quadrants are compressional. Also shown are contours on the Zeit–Shadwan Fault when projected with a planar dip downwards from the surface. Small filled circles are aftershocks of 1969 and 1972, relocated relative to the 1969 mainshock.

probable that the NE-dipping nodal plane in the fault plane solution is the fault plane. Waveform analysis can constrain the NE-dipping fault to having a strike of 300 ± 10°, a dip of 35–40° NE and a rake of −80 to −100° (i.e. almost pure dip slip; see Aki & Richards 1980, p. 106, for the convention defining rake). The nucleation depth of the faulting was in the region of 10 ± 3 km. Details of this seismological analysis are given in the Appendix. The most difficult focal parameter to determine is the epicentre (latitude and longitude of the focus). Routine bulletin locations published by the United States Geological Survey (USGS) or International Seismological Centre (ISC) are known to be in error by up to 15 km for earthquakes of this size (see e.g. Jackson *et al.* 1982). Because the Zeit–Shadwan Fault is the biggest NE-dipping fault in the epicentral region, with the uplift of Shadwan Island attesting to its continuing activity, we think it probable that this was the causative fault of the 1969 earthquake, but cannot be certain. In Fig. 7 we have positioned the 1969 epicentre assuming the earthquake occurred at a depth of 10 km on a planar fault dipping 38° NE that outcrops along the NE coast of Shadwan Island. This is consistent with the seismological observations in the Appendix, with the USGS and ISC locations (Fig. 7), with our knowledge of the geometry of large active normal faults (described earlier) and with the field report of Maamoun & El-Kashab (1978), who also report that west of Shadwan Island a coral reef was apparently uplifted after the earthquake. Such uplift would be expected in the footwall of the Zeit–Shadwan Fault but the report is too imprecise to be easily evaluated.

The second large earthquake occurred on 28 June 1972. This also involved normal faulting with a NW strike. Because it was smaller (Ms 5.6) than the 1969 earthquake its focal parameters are less well resolved (see Appendix); but the NE-dipping plane has a strike of about 310 ± 20°, a dip of 30–40° and a very small (if any) strike-slip component. Its focal depth was again around 10 ± 3 km. By locating this earthquake relative to the 1969 shock (see Jackson & Fitch 1979) the separation between these two events can be found to within about 5 km. The 1972 epicentre is shown in Fig. 7 in a position relative to the 1969 epicentre that was found using this technique. If we fix the 1969 epicentre in our preferred location, then the 1972 epicentre is consistent with a focus at 10 km depth on the Zeit–Shadwan Fault projected downward with a planar dip of 33° from a surface outcrop near Gubal Island. Such an interpretation is consistent with the seismological observations in the Appendix. There were no field reports of the 1972 earthquake. A microearthquake survey by Daggett *et al.* (1986) in 1977 showed intense seismic activity NE of Gubal Island with a concentration of epicentres in a zone trending NW–SE.

In summary, the two earthquakes for 1969 and 1972

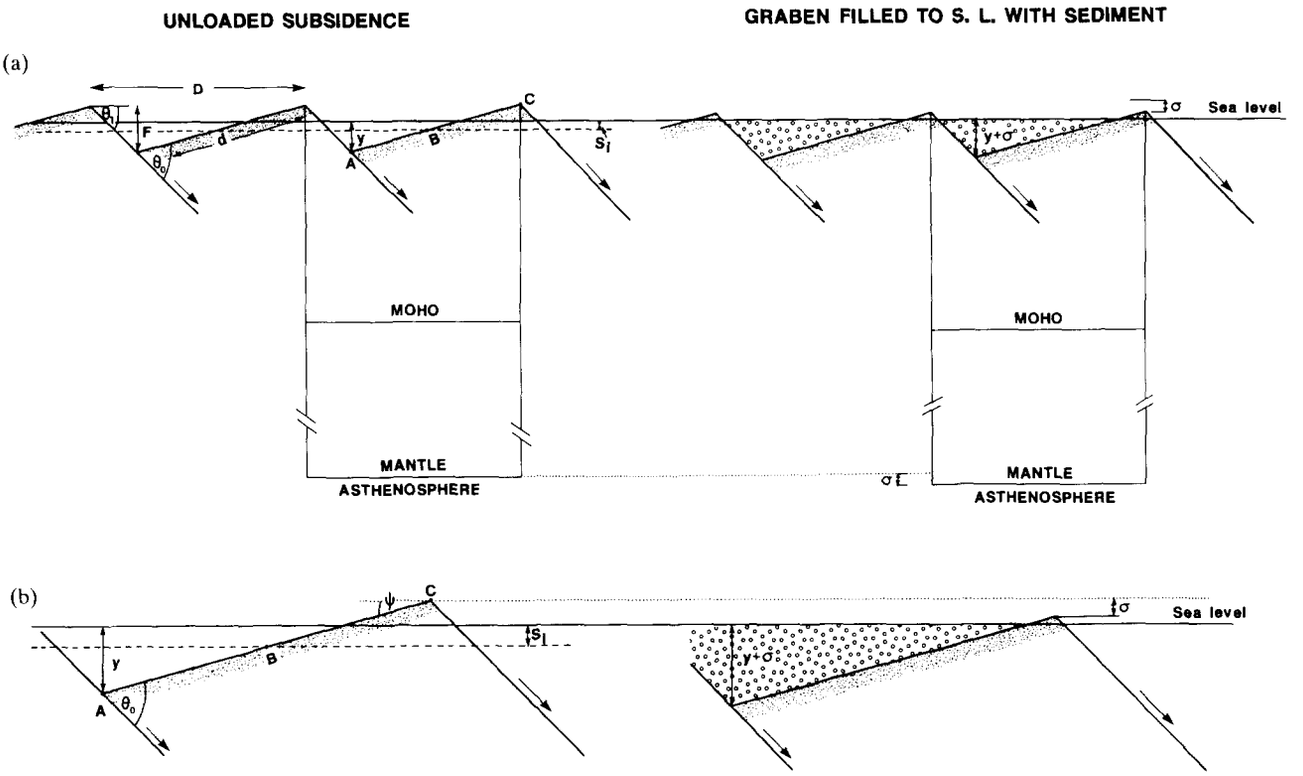

Fig. 8. Cartoons to illustrate the calculation of footwall uplift and graben depth. (a) An initially flat surface (stippled) at sea level is stretched by faulting and tilting and subsides an average of S_i. If the subsidence was in air, the average level passes through point B, where AB = BC. The graben is then filled to sea level with sediment, and the blocks subside an additional amount σ. The two columns shown are assumed to be isostatically balanced. (b) A detail of the upper part of (a).

provide the best direct evidence for the dip of the major NE dipping normal faults in the southern Gulf of Suez. Both involve basement faulting with dips of 30–40° and probably occurred on the Zeit–Shadwan Fault, although this cannot be proved. If they conform to the pattern seen in large active normal faulting earthquakes elsewhere (described earlier), their causative faults were probably approximately planar from the surface to their focal depths. In any case, the faults still dip at 30–40° at a depth of about 10 km, which probably represents the base of the brittle seismogenic upper crust. This dip range of 30–40° is similar to that inferred from drilling data at shallower levels for the Zeit–Shadwan Fault further north, near Gebel Zeit (Letouzey personal communication). We think it probable that, to a first approximation, the Zeit–Shadwan Fault may be considered planar, with a dip of 35 ± 5°, from the surface to a depth of 10 km, an interpretation that is not in conflict with the pattern of large seismogenic normal faults elsewhere in the world (Jackson 1987), that was described earlier.

VERTICAL MOVEMENTS AND NORMAL FAULTING

The model

In this section we will suggest quantitative relations between normal faulting in the 'domino style' (Fig. 1) and vertical movements of the fault-bounded blocks. The model we use is illustrated in Fig. 8 and is conceptually similar to that of Barr (1987a,b) and Yielding (personal communication). We assume that the crust and mantle parts of the lithosphere stretch uniformly (i.e. by the same amount in any particular place), leading to an initial subsidence of the surface of S_i. Superimposed on the new average level of the crustal surface is a saw-tooth topography generated by the normal faulting. We then allow the troughs of this topography to be filled to sea level with sediment, causing an additional subsidence.

We assume that before stretching the surface is at sea level. If stretching occurs in a time short compared to $60/\beta^2$ Ma (where β, the amount of extension, is defined in Fig. 1) then the initial overall subsidence, S_i is given by:

$$S_i = \frac{a\left[(\varrho_m - \varrho_c)\frac{t_c}{a}\left(1 - \frac{\alpha T_1}{2}\frac{t_c}{a}\right) - \frac{\alpha T_1}{2}\varrho_m\right]}{\varrho_m(1 - \alpha T_1)}(1 - 1/\beta) \quad (1)$$

(see McKenzie 1978, Jarvis & McKenzie 1980). Symbols are defined in Table 1. This expression assumes that the basin is unloaded (i.e. contains neither water nor sediment). Substitution of the values in Table 1 reduces (1) to:

$$S_i = 2.46(1 - 1/\beta), \quad (2)$$

where S_i is in km. Superimposed on this average level is a saw-tooth topography of amplitude F between peaks

Table 1. Parameters used in equation (1)

Symbol	Parameters	Value
a	Thickness of lithosphere	125 km
t_c	Thickness of crust	30 km
ϱ_m	Density of mantle (at 0°C)	3.35 g cm^{-3}
ϱ_c	Density of crust (at 0°C)	2.78 g cm^{-3}
ϱ_w	Density of seawater	1.03 g cm
ϱ_a	Density of mantle (asthenosphere) at 1333°C (calculated from ϱ_m and α)	
α	Coefficient of thermal expansion	3.28×10^{-5} °C^{-1}
T_1	Temperature of asthenosphere	1333°C

and troughs created by the faulting (Fig. 8), where $F = d \sin \psi$, $D = d\beta$, $\beta \sin \theta_1 = \sin \theta_0$. θ_0 and θ_1 are the initial and final dips of the faults, d and D are the initial and final horizontal distance between the faults, and $\psi = \theta_0 - \theta_1$ is the amount of tilt (see Jackson & McKenzie 1983).

We now allow the graben to fill to sea level with sediments of density ϱ_s (Fig. 8). This causes an additional subsidence σ, which may be calculated by isostatically balancing the unloaded graben with one filled with sediments to sea level (Fig. 8). Then:

$$\sigma D \varrho_a = \frac{D(y + \sigma)^2 \varrho_s}{2F}, \tag{3}$$

where

$$y = \frac{F}{2} + S_i. \tag{4}$$

The solution to (3) is:

$$\sigma = F\left(\frac{\varrho_a}{\varrho_s}\right) - y \pm \sqrt{F \frac{\varrho_a}{\varrho_s}\left(F \frac{\varrho_a}{\varrho_s} - 2y\right)}, \tag{5}$$

where ϱ_a is the density of the asthenospheric mantle (at 1333°C).

If $y = 0$ (i.e. there is no loading) then σ should be zero, from which it can be seen that the negative value of the square root in (5) is required, i.e.

$$\sigma = F\left(\frac{\varrho_a}{\varrho_s}\right) - y - \sqrt{F \frac{\varrho_a}{\varrho_s}\left(F \frac{\varrho_a}{\varrho_s} - 2y\right)}. \tag{6}$$

The uplift of the footwall crests is then given by

$$U = \frac{F}{2} - S_i - \sigma \tag{7}$$

and the maximum depth of the graben by

$$G = \frac{F}{2} + S_i + \sigma. \tag{8}$$

This assumes that the graben is filled with sediment of uniform density ϱ_s. If compaction is thought to be important, then porosity (ϕ) will vary with depth (z). If we assume an expression of the form

$$\phi = \phi_0 \exp\left(-\frac{z}{\lambda}\right), \tag{9}$$

where ϕ_0 is the initial porosity and λ is a constant (e.g. Sclater & Christie 1980), the average sediment density $\bar{\varrho}$ will vary with depth:

$$\bar{\varrho} = \varrho_s(1 - \phi) + \phi \varrho_w. \tag{10}$$

The sediment load can then be calculated by integration in two dimensions over the cross-sectional area of the triangular graben. The resultant expression for the depth of the graben, G, is then more complicated:

$$G = \frac{1}{F\varrho_a}\left[\frac{1}{2}\varrho_s G^2 - \phi_0 \Delta\varrho\lambda\left\{G - \lambda\left[1 - \exp\left(-\frac{G}{\lambda}\right)\right]\right\}\right] + S_i + \frac{F}{2}, \tag{11}$$

where $\Delta\varrho = \varrho_s - \varrho_w$.The derivation of this expression will be published elsewhere (White N. J., Ph.D. thesis, in preparation). Note that if $\phi_0 = 0$ equation (11) reduces to (8). The value of σ in (6) may be substituted into (8) to provide an initial solution for G that can be used to solve equation (11) by iteration. Convergence is rapid.

If $G > F$ then net subsidence of the footwall crests has occurred and the calculations must be redone as the sediment load is then not triangular but pentagonal in cross-section. In this case the equivalent expression for (11), taken from White N. J., Ph.D. thesis (in preparation), is:

$$G = \frac{1}{F\varrho_a}\left\{\varrho_s F\left(G - \frac{F}{2}\right) - \phi_0 \Delta\varrho\lambda \times \left[F + \lambda \exp\left(-\frac{G}{\lambda}\right)\left\{1 - \exp\left(\frac{F}{\lambda}\right)\right\}\right]\right\} + S_i + \frac{F}{2}. \tag{12}$$

If $G = F$ then (12) reduces to (11). If $\phi_0 = 0$ then (12) reduces to:

$$G = \frac{F}{2} + \left(\frac{\varrho_a}{\varrho_a - \varrho_s}\right) S_i \tag{13}$$

which it should. Equation (13) provides an initial solution to (12), which must also be solved by iteration.

Application to the southern Gulf of Suez

The post-Middle Miocene extension in the Gebel Zeit–Esh Melaha region of the southern Gulf of Suez has evidently caused tilting of about 10° on faults now dipping at about 35°. This suggests an extension, β of about 1.2 in the last 10–15 Ma, which is fast compared to $60/\beta^2$ or 40 Ma, so we are justified in using equation (1) to estimate S_i, providing the extension stretched the crust and mantle equally in any one place.

Figure 9(a) shows the predicted uplift of the footwall crests of Gebel Zeit and Esh Melaha, assuming the geometry sketched in Fig. 4, in which the present day fault dips (θ_1) are in the range 30–40°, the present day spacing between the Esh Melaha and Gebel Zeit Faults (D) is 25 km, and the post-Middle Miocene tilting (ψ) is in the range 5–20°. Two sets of curves are shown, one

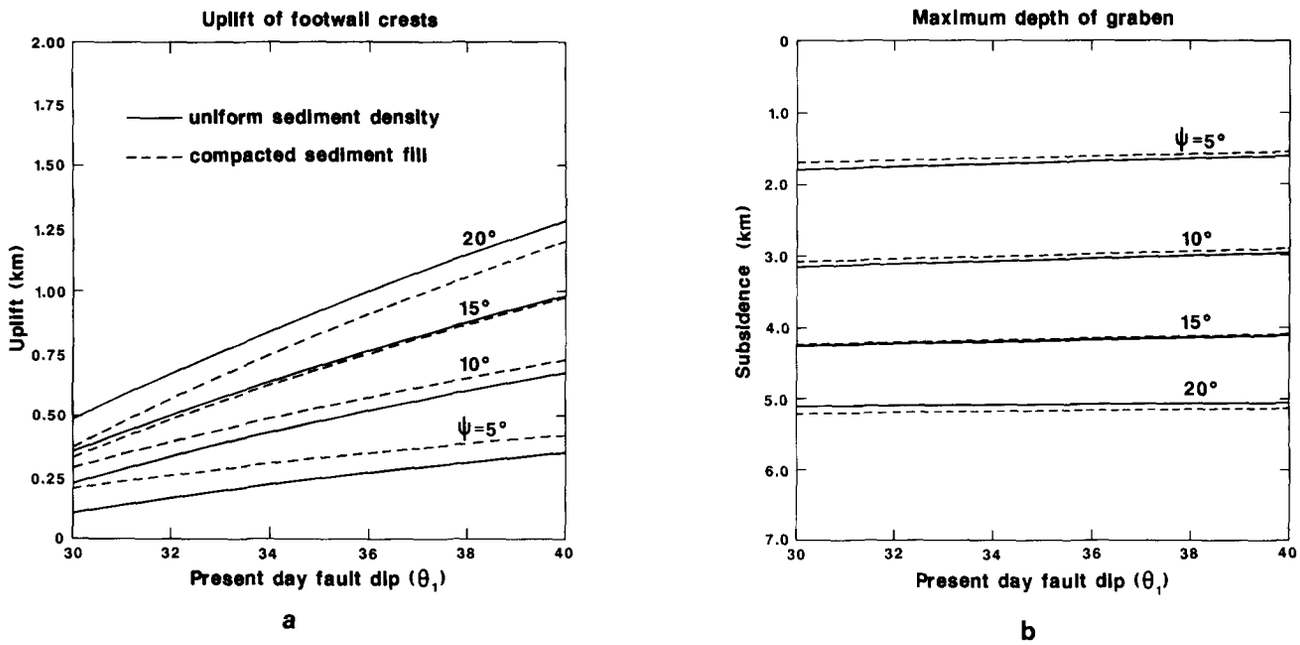

Fig. 9. (a) Footwall uplift and (b) maximum graben depth calculated for the schematic section in Fig. 4, using the model in Fig. 6. Curves are shown for different amounts of tilt (ψ). Two sets of curves are shown, one for sediment fill of uniform density (ϱ_s = 2.0 g cm^{-3}) and the other allowing for compaction, with ϕ_0 = 0.6 and λ = 2 km (see text).

(using equation 6) in which loading is with sediment of a constant density 2.0 g cm^{-3}, the other (using equation 11) in which the density of the solid sediment is 2.5 g cm^{-3} and an initial porosity of 0.6 decays with depth at a rate given by λ = 2 km. Figure 9(b) shows the maximum depth expected for the same Middle Miocene rocks in the grabens.

As discussed earlier, middle Miocene marine rocks occur at elevations of 300 m on Gebel Zeit and may have once covered the whole mountain (elevation 465 m). This amount of uplift is in reasonable agreement with that predicted for faults dipping at 35° with a tilt of 10°. The depth of these same rocks below the Gemsa plain is in the range 3–4 km (Perry 1983, Letouzey personal communication), again in reasonable agreement with Fig. 9. Less is known about the Esh Melaha block. Its highest elevation (431 m) is opposite Gebel Zeit and the topography decays SE along strike. Miocene sediments are only preserved on the ridge crest at the far SE end. These sediments had a clastic source to the NW suggesting that the NW end of the Esh Malaha Ridge was always higher than the SE (El Haddad *et al.* 1984). The thickest sediments in the hangingwall of the Esh Melaha Fault are also in the NW, opposite Gebel Zeit. These observations suggest that the Esh Melaha Fault loses displacement towards the SE and achieved its maximum offset in the NW opposite Gebel Zeit. We do not think that available data can rule out the possibility that the NW part of the Esh Melaha Ridge was covered by the same Middle Miocene sediments seen on Gebel Zeit, and that these sediments were uplifted, tilted by the faulting, and then eroded. That this uplift and tilting in the NW would have been greater than that in the SE of Esh Melaha is not then surprising as the greater amplitude is caused by the greater fault displacement. The surviving basement topography is then a minimum estimate of the uplift experienced by the conjectured sediments on NW Esh Melaha, and is in reasonable agreement with the predictions of Fig. 9.

DISCUSSION

In view of the extreme simplicity of the model we use to estimate vertical motions from the normal faulting and tilting, we are encouraged by the agreement between the observed vertical motions in the southern Gulf of Suez and those predicted in Fig. 9. We chose this part of the Gulf of Suez to illustrate the use of this model because of its apparent simplicity of structure and the availability of sea level, which can act as a horizontal reference level. The main sources of uncertainty in the application of this model to the Gebel Zeit–Esh Melaha region are as follows.

(i) We assume that stretching is uniform and that crust is conserved. In this case the initial subsidence S_i is given by equation (1). Although this is probably the simplest assumption to make, there are cases where the crust may not be conserved during extension. The most likely is when stretching causes partial melting of the mantle and the addition of basalt to the base of the crust. In these circumstances S_i is not correctly predicted by equation (1), and the true value of S_i will be less. In some cases there may even be net uplift rather than subsidence (McKenzie 1984, McKenzie & Bickle in press), i.e. S_i is negative. The magnitude of S_i predicted by equation (2) is in the region of a few hundred metres and is therefore similar to the amount of uplift in Fig. 9(a), so this effect is a matter for concern. Surface basaltic volcanism is a probable sign of magmatic addition to the crust at depth,

but such volcanism is not seen in the southern Gulf of Suez after the Oligocene. We therefore assume that post-Miocene stretching conserved the post-Miocene crust, and that equation (1) applies.

(ii) We assume throughout that sea level has not changed significantly since the Middle Miocene (although this may be uncertain by about ±60 m: see Hallam 1984), that the pre-Middle Miocene topography was approximately at sea level, and that the Middle Miocene sediments of concern to us were deposited at sea level. These assumptions are all questionable, but are probably less important than the other uncertainties. Note, however, that we are assuming a pre-stretching crust with a surface at sea level, and that the uplifted tilted blocks (such as Gebel Zeit) are treated as emergent footwall islands. In other circumstances, a different starting configuration may be appropriate (e.g. Barr 1987b).

(iii) Our analysis assumes that all the observed vertical movements result from faulting and extension in the manner of Fig. 8. In fact a regional uplift of the entire Gulf of Suez and Sinai areas may be important (e.g. Moretti & Froidevaux 1986, Moretti *et al.* 1987), as may some regional subsidence caused by the decay of a thermal anomaly related to the pre-Middle Miocene extensional event.

(iv) The calculated amplitude of the footwall uplift is sensitive to the density of the sediment that infills the grabens. Our chosen values for the average sediment density (2.0 g cm^{-3}), solid sediment density (2.5 g cm^{-3}) and λ (2 km) are only rough estimates. Since the entire graben fill is being considered they are probably reasonable. Nevertheless, the properties of the sediment fill are certainly the most important source of error: changing the average sediment density by 10% (to 1.8 or 2.2 g cm^{-3}) can change the uplift of the footwall crests in Fig. 9(a) by 200 m.

(v) The rotating blocks ('dominoes') are treated as rigid and bounded by planar faults. This is almost certainly an over-simplification. Any difference in tilt either side of the major fault requires either some fault curvature in cross-section or internal deformation of the fault bounded blocks. Moreover, even the best earthquake data cannot exclude a fault curvature in cross-section of up to 10–15°. To quantify the effects of non-rigidity and minor fault curvature would require a far more complicated model that is not justified by the present observations.

In spite of these uncertainties, our analysis suggests that the simple model in Fig. 8 can predict the approximate amplitude of the vertical movements associated with tilting and normal faulting in the southern Gulf of Suez. Such movements are important. The uplift of footwall crests dominates the geomorphology, and hence drainage and distribution of sedimentary facies. The depth of burial of sediments in hangingwall grabens will strongly influence potential source rock maturity. The model used here is not unique, but it is simple and compatible with both the observed fault geometry and our knowledge of how normal faults work. Other models

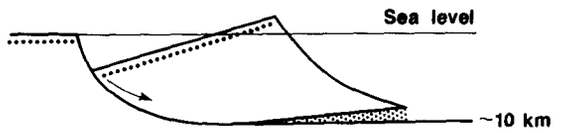

Fig. 10. An alternative model to explain uplift of the Gebel Zeit block, by rotational movement of the hangingwall block on a strongly curved (listric) fault above a rigid footwall. The stippled 'void' at depth is assumed to be filled by internal deformation of the hangingwall block (after Moretti & Colletta, 1988).

are available: for example Moretti & Colletta (1987, 1988) suggest that the uplift of Gebel Zeit results from the rotation of the hangingwall block on a strongly curved listric fault that becomes horizontal at a depth (10 km) that marks the brittle–ductile transition in the crust (Fig. 10). This interesting alternative geometry is incompatible with earthquake data, which suggest that at 10 km the large normal faults in the southern Gulf of Suez are still dipping at about 35°. In addition, their geometry is unlike that seen in large seismic normal faults elsewhere in the world, which appear to be approximately planar and cut right through the brittle upper crust. They do not appear to flatten out at the brittle–ductile transition.

CONCLUSIONS

We have attempted to see whether our current understanding of how large seismogenic normal faults move can be used to help predict the amplitudes of the fault-controlled vertical movements in extensional terrains. Such movements often dominate the syn-rifting sedimentary history of extensional basins and are important for the maturation of sediments at deeper levels in fault-bounded tilted blocks. We investigate a model, similar to that of Barr (1987a, b) and Yielding (personal communication), in which overall subsidence is caused by lithospheric and crustal extension (McKenzie 1978). Superimposed on this subsidence is a saw-tooth topography generated by large normal faults that are planar throughout the brittle upper crust and rotate as they move. We assume that the fault-bounded grabens are always filled to sea level with sediment.

This model was then applied to the southern Gulf of Suez, where earthquakes demonstrate that normal faulting at a dip of about 35° extends to around 10 km depth. Middle Miocene rocks are uplifted to about 300–500 m above sea level in the footwalls of active faults and are also found at depths of 3–4 km in the intervening grabens. These observed vertical movements are in reasonable agreement with those predicted by the model, in spite of various uncertainties. We conclude that the model is useful for predicting vertical motions in extensional terrains. Its virtues are (a) its simplicity and (b) its compatibility with our knowledge of how large active normal faults move. This study emphasizes how rather small tilts can lead to large vertical motions in extensional terrains, if the fault-bounded blocks are wide enough.

Acknowledgements—We are grateful to G. Yielding and D. Barr for first bringing this model to our attention, and D. Barr for a preprint of his paper. J. A. Jackson would like to thank J. Hurst and R. Graham for useful discussions in the field, Dr R. Kebeasy for logistical help and R. Westaway for help with the SH synthetic seismograms. Many people know far more about the Gulf of Suez then we do. We would especially like to thank J. Letouzey, P. Chenet, R. Graham, J. Hurst and I. Vann for patiently correcting our misconceptions and for other help, although they do not necessarily agree with our interpretations. All of the above, and S. Perry, I. Moretti and B. Colletta (who kindly sent us several preprints), stimulated our interest greatly. This work was partly supported by NERC and is contribution No. 1039 of Cambridge University, Department of Earth Sciences.

REFERENCES

Aissaoui, D. M., Coniglio, M., James, N. P. & Purser, B. H. 1986. Diagenesis of a Miocene Reef-platform: Jebel Abu Shaar, Gulf of Suez, Egypt. In: *Reef Diagenesis* (edited by Schroeder, J. H. & Purser, B. H.). Springer-Verlag, Berlin.

Aki, K. & Richards, P. G. 1980. *Quantitative Seismology*. Freeman, San Francisco.

Angelier, J. 1985. Extension and rifting: the Zeit region, Gulf of Suez. *J. Struct. Geol.* **7**, 605–612.

Barr, D. 1987a. Lithosphere stretching, detached normal faulting and footwall uplift. In: *Continental Extensional Tectonics* (edited by Coward, M. P., Dewey, J. F. & Hancock, P. L.). *Spec. Publs geol. Soc. Lond.* **28**, 75–94.

Barr, D. 1987b. Structure/stratigraphic models for extensional basins of half graben type. *J. Struct. Geol.* **9**, 491–500.

Ben-Menahem, A. & Aboodi, E. 1971. Tectonic patterns in the Northern Red Sea region. *J. geophys. Res.* **76**, 2764–2689.

Chen, W. P. & Molnar, P. 1983. Focal depths of intracontinental and intraplate earthquakes and their implications for the thermal and mechanical properties of the lithosphere. *J. Geophys. Res.* **88**, 4183–4214.

Chenet, P.-Y., Colletta, B., Letouzey, J., Desforges, G., Ousset, E. & Zaghloul, E. A. 1985. Geological structures associated with extensional tectonics in the Suez rift. Institute Francais du Petrole, report B4181001.

Chenet, P.-Y. & Letouzey, J. 1983. Tectonique de la zone comprise entre Abu Durba et Gebel Mezzazat (Sinai, Egypte), dans le contexte de l'evolution du rift de Suez. *Bull. Centres Rech. Explor. Prod. Elf-Aquitaine* **7**, 201–215.

Colletta, B., Moretti, I. Chenet, P.-Y., Muller, C. & Gerard, P. In press. The structure of the Gebel Zeit area: a field example of tilted block crest in the Suez rift. *Proc. 8th E.G.P.L. Explor. Seminar.*

Crossland, C. 1939. Chapters 1 (Narrative and list of stations) and 3 (Some Coral Formations). In: *Reports on the Preliminary Expedition for the Exploration of the Red Sea in the R.R.S. Mabahith.* Publ. Mar. Biol. Station Ghardaga (Red Sea), **1**, 1–11, 21–35.

Daggett, P. H., Morgan, P., Boulos, F. K., Hennin, S. F., El-Sherif, A. A., El-Sayed, A. A., Basta, N. Z. & Melek, Y. S. 1986. Seismicity and active tectonics of the Egyptian Red Sea margin and northern Red Sea. *Tectonophysics* **125**, 313–324.

El-Haddad, A., Aissaoui, D. M. & Soliman, M. A. 1984. Mixed carbonate-siliciclastic sedimentation on a Miocene fault block, Gulf of Suez, Egypt. *Sed. Geol.* **37**, 185–202.

England, P. C. & Jackson, J. A. 1987. Migration of the seismic–aseismic transition during uniform and non-uniform extension of the continental lithosphere. *Geology* **15**, 291–294.

Eyidoğan, H. & Jackson, J. 1985. A seismological study of normal faulting in the Demirci, Alaşehir and Gediz earthquakes of 1969–1970 in western Turkey: implications for the nature and geometry of deformation in the continental crust. *Geophys. J. R. astr. Soc.* **81**, 569–607.

Garfunkel, Z. & Bartov, Y. 1977. The tectonics of the Suez rift. *Geol. Surv. Israel Bull.* **71**.

Garrison, L. E. & Martin, R. G. 1973. Geologic structures in the Gulf of Mexico basin. *Prof. Paper U.S. Geol. Surv.* **773**, 1–85.

Gibbs, A. D. 1984. Structural evolution of extensional basin margins. *J. geol. Soc. Lond.* **141**, 609–620.

Hallam, A. 1984. Pre-Quaternary sea-level changes. *Annu. Rev. Earth Planet. Sci.* **12**, 205–243.

Huang, P. Y. & Solomon, S. C. 1987. Centroid depths and mechanisms of mid-ocean ridge earthquakes in the Indian Ocean, Gulf of Aden, and Red Sea *J. geophys. Res.* **92**, 1361–1382.

Jackson, J. A. 1987. Active normal faulting and continental extension. In: *Continental Extensional Tectonics* (edited by Coward, M. P., Dewey, J. F. & Hancock, P. L.). *Spec. Publs geol. Soc. London.* **28**, 3–17.

Jackson, J. A. & Fitch, T. J. 1979. Seismotectonic implications of relocated aftershock sequences in Iran and Turkey. *Geophys. J. R. astr. Soc.* **57**, 471–482.

Jackson, J. A., Gagnepain, J., Houseman, G., King, G., Papadimitriou, P., Soufleris, C. & Virieux, J. 1982. Seismicity, normal faulting and the geomorphological development of the Gulf of Corinth (Greece): the Corinth earthquakes of February and March 1981. *Earth Planet. Sci. Lett.* **57**, 377–397.

Jackson, J. A. & McKenzie, D. 1983. The geometrical evolution of normal fault systems. *J. Struct. Geol.* **5**, 471–482.

Jackson, J. A. & McKenzie, D. 1984. Active tectonics of the Alpine-Himalayan belt between Turkey and Pakistan. *Geophy. J. R. astr. Soc.* **77**, 185–264.

Jankhof, K. 1945. Changes in ground level produced by the earthquakes of April 14 and 18 1928 in southern Bulgaria. In: *Tremblements de Terre en Bulgarie*, Nos. 29–31, Institut Meteorologique central de Bulgarie, Sofia, 131–136 (in Bulgarian).

Jarvis, G. T. & McKenzie, D. P. 1980. Sedimentary basin formation with finite extension rates. *Earth Planet. Sci. Lett.* **48**, 42–52.

Langston, C. A. & Helmberger, D. V. 1975. A procedure for modelling shallow dislocation sources. *Geophys. J. R. astr. Soc.* **42**, 117–130.

Maamoun, E. S. & El-Kashab, H. M. 1978. Seismic studies of the Shadwan (Red Sea) earthquake. *Helwan Inst. Astron. Geophys. (Egypt) Bull.* **171**, 28.

McKenzie, D. P. 1978. Some remarks on the development of sedimentary basins. *Earth Planet. Sci. Lett.* **40**, 25–32.

McKenzie, D. P. 1984. A possible mechanism for epirogenic uplift. *Nature Lond.* **307**, 616–618.

McKenzie, D. P. & Bickle, M. J. In press. The volume and composition of melt generated by extension of the lithosphere. *J. Petrol.*

Meissner, R. & Strehlau, J. 1982. Limits of stress in continental crusts and their relation to depth–frequency distribution of shallow earthquakes. *Tectonics* **1**, 73–89.

Moretti, I., Chenet, P.-Y. & Colletta, B. 1987. The narrowing of the Suez rift: a combination of stretching and secondary convection. *Tectonophysics* **133**, 229–234.

Moretti, I. & Colletta, B. 1988. Fault-block tilting: the Gebel Zeit example, Gulf of Suez. *J. Struct. Geol.* **10**, 9–20.

Moretti, I. & Froidevaux, C. 1986. Thermochemical models of active rifting. *Tectonics* **5**, 501–511.

Moretti, I. & Froidevaux, C. 1986. Thermomechanical models of active rifting. *Tectonics* **5**, 501–511.

Myers, W. B. & Hamilton, W. 1964. Deformation accompanying the Hebgen Lake earthquake of August 17 1959. *Prof. Pap. U.S. Geol. Surv.* **435**, 55–98.

Perry, S. K. 1983. The geology of the Gebel Zeit region: Gulf of Suez, Egypt. Earth Sciences and Resources Institute, University of South Carolina, Occasional Pub. 2.

Ransome, F. L., Emmons, W. H. & Garrey, G. H. 1910. Geology and ore deposits of the Bullfrog District, Nevada. *U.S. Geol. Surv. Bull.* **407**, 1–130.

Richter, C. F. 1958. *Elementary Seismology*. W. H. Freeman, San Francisco.

Robson, D. A. 1971. The structure of the Gulf of Suez (Clysmic) Rift, with special reference to the eastern side. *Q. Jl geol. Soc. Lond.* **115**, 41–47.

Said, R. 1962. *The Geology of Egypt*. Elsevier, Amsterdam.

Savage, J. C. & Hastie, L. M. 1966. Surface deformation associated with dip slip faulting. *J. geophys. Res.* **71**, 4897–4904.

Scholz, C. H. 1982. Scaling laws for large earthquakes: consequences for physical models. *Bull. seism. Soc. Am.* **72**, 1–14.

Sclater, J. G. & Christie, P. A. F. 1980. Continental stretching: an explanation of the post mid-Cretaceous subsidence of the Central North Sea basin. *J. geophys. Res.* **85**, 3711–3739.

Selwood, B. W. & Netherwood, R. E. 1984. Facies evolution in the Gulf of Suez area: sedimentation history as an indicator of rift initiation and development. *Modern Geol.* **9**, 43–69.

Shimazaki, K. 1986. Small and large earthquakes: the effects of the thickness of seismogenic layer and the free surface. In: *Earthquake Source Mechanics*, Maurice Ewing Series, Vol. 6 (edited by Das, S., Boatwright, J. & Scholz, C. H.). *Am. geophys. Un.*, 209–216.

Shukri, N. M. 1954. The geology of Shadwan Island, northern Red Sea. *Bull. Soc. Geogr. d'Egypte* **27**, 83–92.

Sibson, R. H. 1982. Fault zone models, heat flow, and the depth

distribution of earthquakes in the continental crust of the United States. *Bull. seism. Soc. Am.* **72**, 151–163.
Soufleris, C. & Stewart, G. S. 1981. A source study of the Thessaloniki (Northern Greece) earthquake sequence. *Geophys. J. R. astr. Soc.* **67**, 343–358.
Steckler, M. 1986. Uplift and extension at the Gulf of Suez—indication of induced mantle convection. *Nature Lond.* **317**, 135–139.
Stein, R. S. & Barrientos, S. E. 1985. Planar high angle faulting in the Basin and Range: Geodetic analysis of the 1980 Borah Peak, Idaho earthquake. *J. geophys. Res.* **90**, 11, 355–11, 366.
Stewart, J. H. 1980. Regional tilt patterns of late Cenozoic basin-range fault blocks, western United States. *Bull. geol. Soc. Am.* **91**, 460–464.
Strehlau, H. 1986. A discussion of the depth extent of rupture in large continental earthquakes. In: *Earthquake Source Mechanisms*, Maurice Ewing Series, Vol. 6 (edited by Das, S., Boatwright, J. & Scholz, C. H.). *Am. geophys. Un.*, 131–145.
Westaway, R. & Jackson, J. A. 1987. The earthquake of 23 November 1980 in Campania–Basilicata (Southern Italy). *Geophys. J. R. astr. Soc.* **90**, 375–443.

APPENDIX

SOURCE GEOMETRIES OF THE 31 MARCH 1969 AND 28 JUNE 1972 EARTHQUAKES

The modelling of long period P and SH waveforms using synthetic seismograms has become a standard technique for determining the source orientation, depth and seismic moment of earthquakes. The method was first described by Langston & Helmberger (1975) and has become too routine to justify detailed description here; the reader is referred to Soufleris & Stewart (1981) for greater detail. The earthquake is represented by a point source of finite duration, described by a trapezoidal time function with a rise, a plateau and a fall time. Teleseismic P waveforms in the epicentral distance range 30–85° are modelled by the interference between the direct P wave and the surface reflections pP and sP. Teleseismic SH waveforms are assumed to consist of direct S waves and the surface reflection sS. The amplitudes of these phases are controlled by the source orientation, which can be varied within the constraints of the first motion polarities in the fault plane solution. The rays are then combined with an instrument response and an attenuation operator to produce synthetic seismograms at various focal depths. These are then compared with the observed seismograms. All the seismograms used here were observed on long period instruments of the World Wide Standard Seismograph Network (WWSSN). We assumed a P velocity of 6 km s^{-1} above the source and 6.8 km s^{-1} below, with an S velocity of $1/\sqrt{3}$ times the P velocity.

The 1969 *mainshock*

The waveforms from this shock were simple and characteristic of a shallow normal faulting event (Fig. A1). The first motion polarities and waveforms strongly constrain the source orientation of this shock. The waveforms for our preferred solution (Table A1) are also shown in Fig. 10. Our results are very close to, and within the error bounds of, a formal inversion for the source of this earthquake performed by Huang & Solomon (1987), also shown in Table A1. The differences betweeen the two are not significant. An earlier solution for the source of this earthquake by Ben-Menahem & Aboodi (1971), who used surface waves and found a larger strike-slip component, is not compatible with the observed body waves. Our estimate of uncertainty in the 10 km focal depth is about ±3 km. Huang & Solomon (1987) suggest that faulting probably extends from the surface to about twice their centroidal depth.

Table A1. Earthquake source parameters

	This study	Huang & Solomon (1987)
31 March 1969		
Origin time	07:15:54 (ISC)	
m_b	6.1 (ISC)	
M_s	6.8 (ISC)	
Mo (10^{17} Nm)	180	110
strike	304°	294° (285–310°)
dip	38°	37° (35–40°)
rake	−85°	−89° (−80–−110°)
depth (km)	10	6.2 (5.5–8.0)
Time function (total duration, sec)	8.0	9.5
28 June 1972		
Origin time	09:49:36 (ISC)	
m_b	5.5 (ISC)	
M_s	5.5 (ISC)	
Mo (10^{17} Nm)	4.7	3.7
strike	322°	288° (260–300°)
dip	30°	40° (30–50°)
rake	−80°	−100° (−60–−130°)
depth (km)	10	6.1 (5.0–11.0)
Time function (sec)	4.0	4.0

ISC—the International Seismological Centre. Values in parantheses are the ranges estimated from Huang & Solomon's inversion. The convention for strike, dip and rake is that of Aki & Richards (1980).

The 1972 *mainshock*

Although numerous first motion polarities are available for this shock, it was smaller than the 1969 event and the waveform data are less good. Our results (Fig. A2 and Table A1) are similar to those of Huang & Solomon (1987) and generally within their error bounds, though our preferred strike (322°) differs from theirs (288°) by 34°, because theirs is incompatible with first motion data. Both solutions require dominantly normal faulting with an orientation at depth similar to that of the 1969 shock. Note that the mechanism in Fig. A2 differs slightly from that of Jackson & McKenzie (1984) who mistakenly read the P wave onset at AAE as compressional, when in fact a small downward pulse precedes the upward compression on the long period WWSSN instrument.

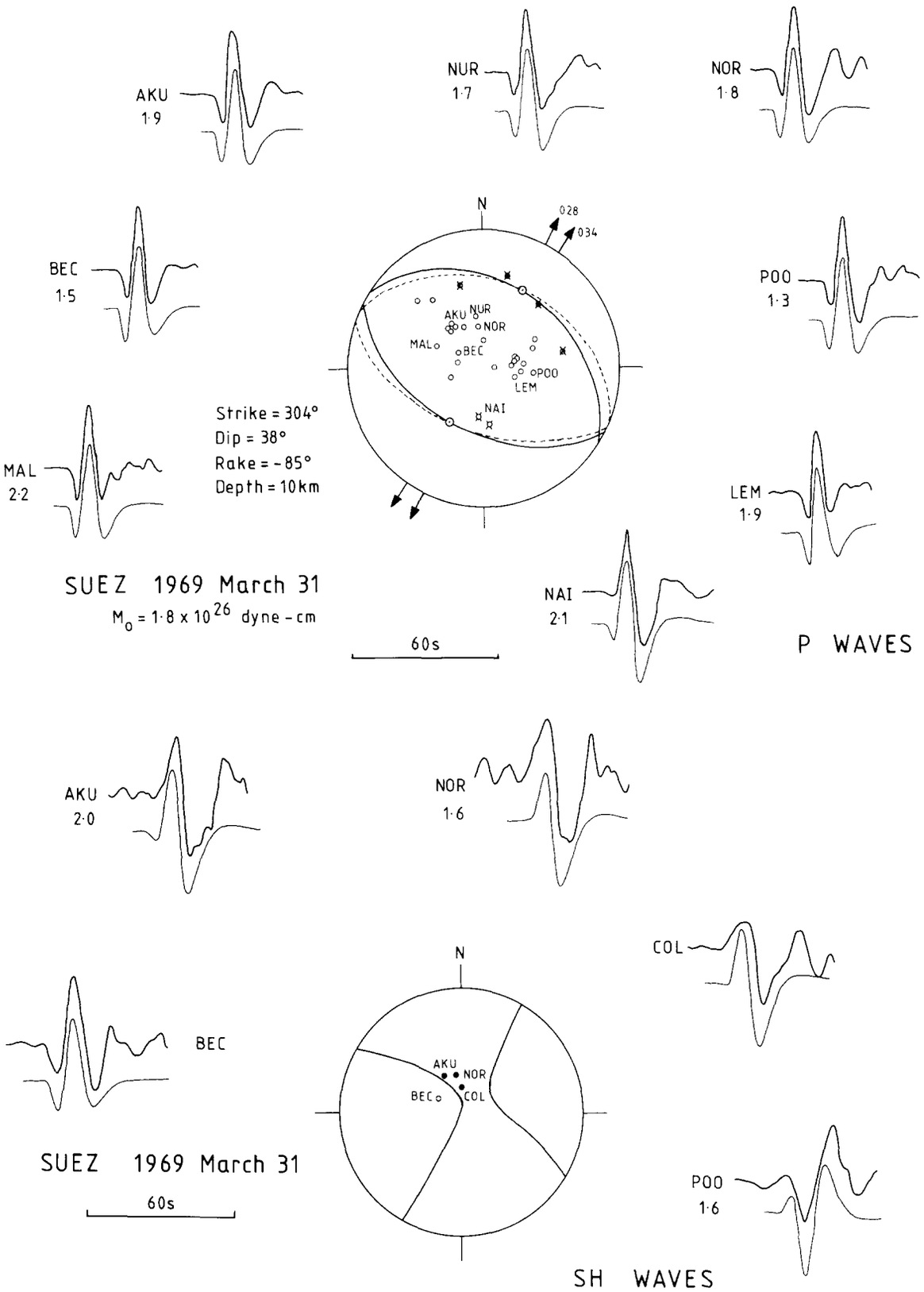

Fig. A1. Seismological observations for the 1969 mainshock. Observed (top) and synthetic (bottom) long period WWSSN seismograms are shown for our preferred focal mechanism (Table A1). The upward direction is compressional. Equal-area lower hemisphere focal spheres and nodal planes are shown for P and SH waves. Solid nodal planes are ours, dashed planes on the P wave focal sphere are those from Huang & Solomon (1987). Numbers next to stations are moment estimates in units of 10^{19} Nm (10^{26} dyne cm).

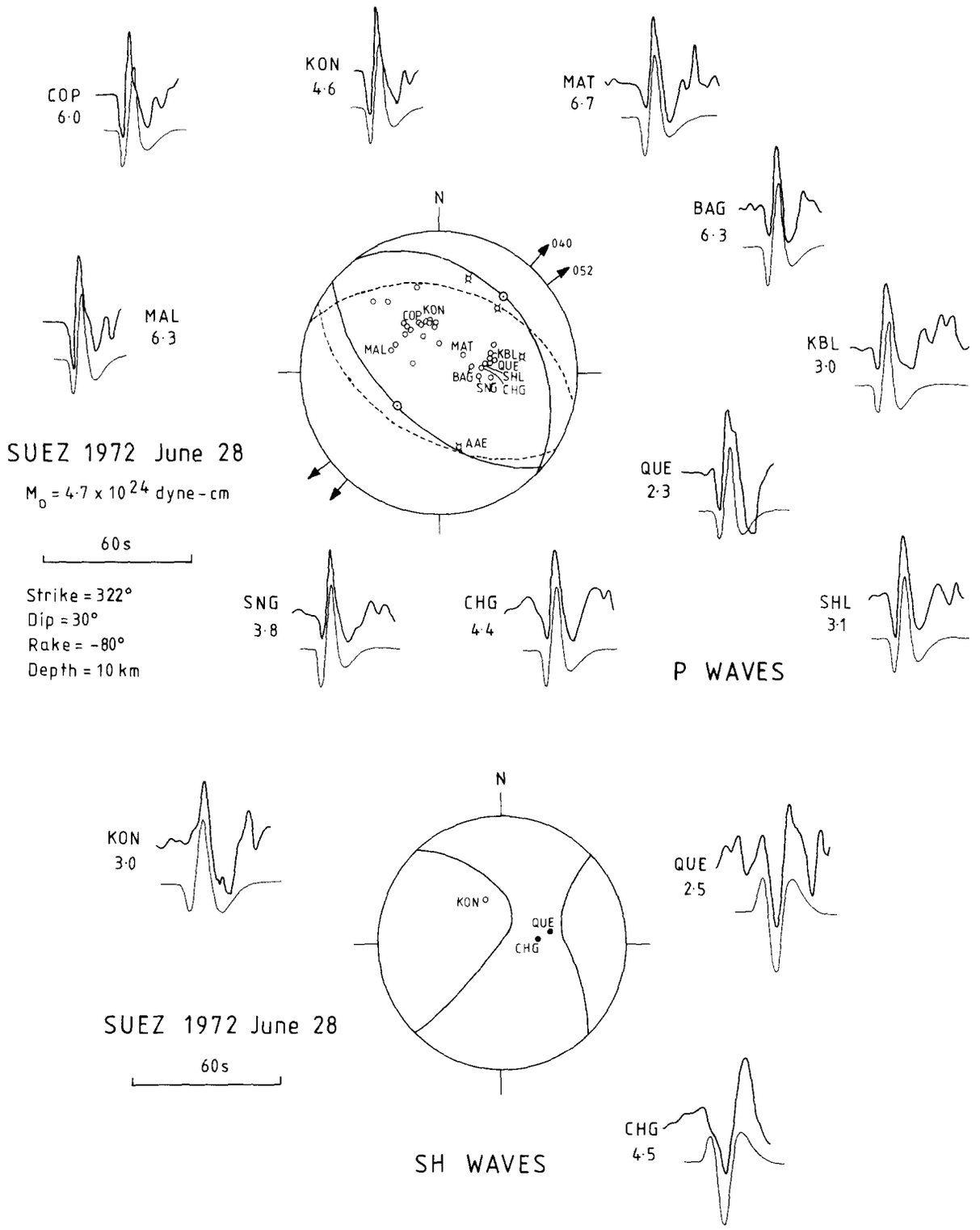

Fig. A2. Seismological observations for the 1972 mainshock. Symbols as in Fig. A1. Moments are in units of 10^{17} Nm (10^{24} dyne cm).